CHAPTER 8

DOUBLE-DIFFUSIVE CONVECTION

A comparatively recent development in the field of convection has been the study of fluids in which there are gradients of two (or more) properties with different molecular diffusivities. When the concentration gradients have opposing effects on the vertical density distribution, a number of surprising things can happen, and these are the subject of the present chapter. The phenomena were first studied with an application to the ocean in mind (see §8.2.4), and because heat and salt (or some other dissolved substance) are then the relevant properties, the process has been called 'thermohaline' or 'thermosolutal' convection. Related effects have now been observed in the laboratory using a pair of solutes, and in solidifying metal alloys, and the name 'double-diffusive convection' has been chosen to encompass this wider range of phenomena.

The stability problem will first be reviewed, somewhat more fully than was done in previous chapters because of the comparative novelty of the double-diffusive phenomena. It will then be shown that when two components contribute to the vertical density gradient, a series of steps tends to form, with well-mixed layers separated by sharper density interfaces. The detailed structure of these interfaces and measurements of the coupled fluxes across them will also be described.

8.1. The stability problem

8.1.1. *The mechanism of instability*

In such a system with opposing gradients, the existence of a net density distribution which decreases upwards is *not* a guarantee of stability. Diffusion, which was seen in §7.1.1 to be generally stabilizing in a fluid containing a single solute, can now act so as to allow the release of the potential energy in the component which is

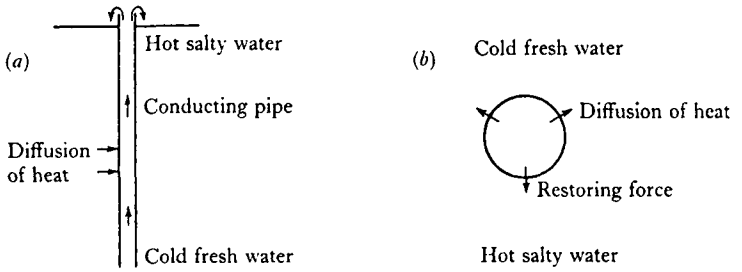

Fig. 8.1. Illustrating the two types of motion which are possible in a fluid containing opposing vertical gradients of heat and salt (*a*) salt fountain, (*b*) oscillating element.

heavy at the top. The form of the motions depends on whether the driving energy comes from the substance of higher or lower diffusivity, and our physical intuition based on observations of ordinary thermal convection is of little direct help here. Two simple conceptual experiments (the first of which was the starting point of the whole subject) do bring out the main features of the two possible kinds of motion.

Consider first, following Stommel, Arons and Blanchard (1956), a long narrow heat-conducting pipe inserted vertically through a region of the ocean where warm salty water overlies colder fresher (and of course denser) water (fig. 8.1 *a*). Water which is pumped upwards, say, would quickly reach the same temperature as the surroundings at the same level (by conduction of heat through the wall of the pipe), while it remains fresher and therefore lighter. A 'salt fountain' started in this way (in either direction) will continue to flow so long as there is a vertical gradient of salinity to supply potential energy. Some confusion (mostly semantic) has arisen in describing the role of heat in this case. The temperature distribution is stabilizing in the sense that initially the warmer water is on top, but the diffusion of heat is the essential destabilizing process.

In the opposite case (of warm salty water underneath colder, fresher, lighter water) consider a parcel of fluid which is isolated from its surroundings by a thin conducting shell and then displaced upwards (fig. 8.1 *b*). It will lose heat but not salt, and buoyancy forces must drive it back towards its initial position. In this way an oscillatory motion will be produced, with the buoyancy reversing each

half cycle and the parcel overshooting its position of neutral equilibrium. Any lag in temperature between the moving fluid and its surroundings implies that there is a net buoyancy force in the direction of motion over much of the cycle, and so the oscillations can grow even when some energy is dissipated.

A most important step forward was taken by Stern (1960), who pointed out that solid boundaries are not essential to the above arguments. A slower transfer of salt relative to heat is assured by its smaller molecular diffusivity, and motions of both the kinds described above can be set up in the interior of a fluid. In the first case, long narrow convecting cells, called 'salt fingers', have been predicted and observed (see fig. 8.8 pl. xx), and in the second, the existence of oscillatory motions has been verified. For reasons which will become clearer in §8.2, these two will be distinguished by calling them the 'finger' and 'diffusive' regimes respectively. Some of their properties can be derived using the stability analysis described in the following section. The extent to which these simple predictions need modification to describe the fully developed convection phenomena will be discussed in conjunction with laboratory observations.

8.1.2. *Linear stability analysis*

Only the simplest case will be described here, the stability to infinitesimal disturbances of a system containing linear opposing gradients of two properties, with free horizontal boundaries above and below held at fixed concentrations (temperatures and salinities). This problem was treated by Stern (1960), but we now add the restriction of two-dimensional motion and incorporate further results due to Veronis (1965) and Baines and Gill (1969). Stability criteria for a wide variety of conditions at the boundaries have been obtained by Nield (1967) and for the case of an unbounded fluid by Walin (1964). These make a small quantitative difference to the values of the critical parameters, but introduce no new qualitative effects.

The density distribution can be written in the linear approximations as

$$\rho = \rho_{\mathrm{m}}(1 - \alpha T^* + \beta S^*), \tag{8.1.1}$$

where ρ_{m} is the mean density at height z_* (which is assumed to vary

linearly between $z_* = 0$ and $z_* = d$). T^* is the temperature, or more generally the concentration of the property with higher molecular diffusivity, and S^* is the salinity (concentration of the component with lower diffusivity): α and β are the corresponding 'coefficients of expansion' defined in such a way that they are both positive for temperature and salinity changes at constant pressure

$$\alpha = -\frac{1}{\rho}\left(\frac{\partial \rho}{\partial T^*}\right)_{S^*, p^*}, \quad \beta = \frac{1}{\rho}\left(\frac{\partial \rho}{\partial S^*}\right)_{T^*, p^*}. \tag{8.1.2}$$

The linearized two-dimensional Boussinesq equations (1.3.10) can be reduced to the dimensionless form (scaling with d and κ, and introducing dimensionless parameters to be defined below)

$$\left(\frac{1}{Pr}\frac{\partial}{\partial t} - \nabla^2\right)\nabla^2\psi = -Ra\frac{\partial T}{\partial x} + Rs\frac{\partial S}{\partial x}. \tag{8.1.3}$$

The diffusion equations for the two components, with similar scaling, are

$$\left.\begin{aligned}\left(\frac{\partial}{\partial t} - \nabla^2\right)T &= -\frac{\partial \psi}{\partial x},\\ \left(\frac{\partial}{\partial t} - \tau\nabla^2\right)S &= -\frac{\partial \psi}{\partial x},\end{aligned}\right\} \tag{8.1.4}$$

where ψ is a stream function, defined as before, and the non-dimensional T and S have been defined relative to the mean linear gradients. The boundary conditions at $z = z_*/d = 0, 1$ become

$$\psi = 0, \quad \partial^2\psi/\partial z^2 = 0, \quad T = S = 0. \tag{8.1.5}$$

With the introduction of two independent concentration differences ΔT and ΔS between the bottom and top boundaries, and two different molecular diffusivities, four non-dimensional parameters are needed to specify the system completely. In addition to $Ra = g\alpha\Delta T d^3/\kappa\nu$ and $Pr = \nu/\kappa$ used earlier, the above equations contain $\tau = \kappa_S/\kappa < 1$, the ratio of diffusivities, and the density ratio $\beta\Delta S/\alpha\Delta T$. The latter can be replaced by an equivalent 'salinity Rayleigh number' Rs such that

$$Rs = \frac{\beta\Delta S}{\alpha\Delta T}Ra = \frac{g\beta\Delta S d^3}{\kappa\nu} \tag{8.1.6}$$

(but note that κ, not κ_S, appears in the denominator here).

Rather than eliminating two of the variables to give a single equation in the third (the procedure implied by the form of (7.1.6) quoted earlier), the boundary conditions (8.1.5) are such that one can write down directly a set of functions satisfying (8.1.3) and (8.1.4):

$$\left.\begin{aligned} \psi &\sim \mathrm{e}^{pt}\sin \pi a x \cdot \sin \pi n z, \\ T, S &\sim \mathrm{e}^{pt}\cos \pi a x \cdot \sin \pi n z, \end{aligned}\right\} \tag{8.1.7}$$

where πa and πn are horizontal and vertical wavenumbers; n must be an integer but a is so far unrestricted. The characteristic equation derived by substitution is a cubic in p,

$$p^3+(Pr+\tau+1)k^2p^2+[(Pr+\tau Pr+\tau)k^4-(Ra-Rs)Pr\pi^2a^2/k^2]p \\ +\tau Prk^6+(Rs-\tau Ra)Pr\pi^2a^2=0, \tag{8.1.8}$$

where $k^2=\pi^2(a^2+n^2)$.

The subsequent infinitesimal motion is described by the solutions of (8.1.8) for various combinations of parameters. (See Baines and Gill (1969) for a detailed discussion, especially of the case $Pr = 10$, $\tau = 10^{-2}$ which corresponds roughly to salt and heat in water.) At least one value of p must be real, but $p = p_r + ip_i$ is in general a complex number whose real part represents the growthrate, and whose imaginary part allows for an oscillatory behaviour. For fixed Prandtl number Pr and fixed τ, the stability boundaries (minimum Ra with $p_r = 0$) correspond to two straight lines in the Ra, Rs plane whose equations are

$$\left.\begin{aligned} XZ\text{:}\quad & Ra=\frac{Rs}{\tau}+\frac{27\pi^4}{4}, \\ XW\text{:}\quad & Ra=\frac{Pr+\tau}{Pr+1}Rs+(1+\tau)\left(1+\frac{\tau}{Pr}\right)\frac{27\pi^4}{4}. \end{aligned}\right\} \tag{8.1.9}$$

These are drawn, diagrammatically and not to scale, in fig. 8.2.

In the quadrant where Ra is negative and Rs positive, both gradients are stabilizing and no growth is possible. In the opposite (upper left) quadrant, all points are unstable above XZ, so that $Ra_e \equiv Ra - Rs/\tau = \frac{27}{4}\pi^4$ represents an effective Rayleigh number having the same role as Ra_c in ordinary convection; Ra_e reduces to Ra_c when either component is present alone, and the numerical values also vary with the boundary conditions in the same way.

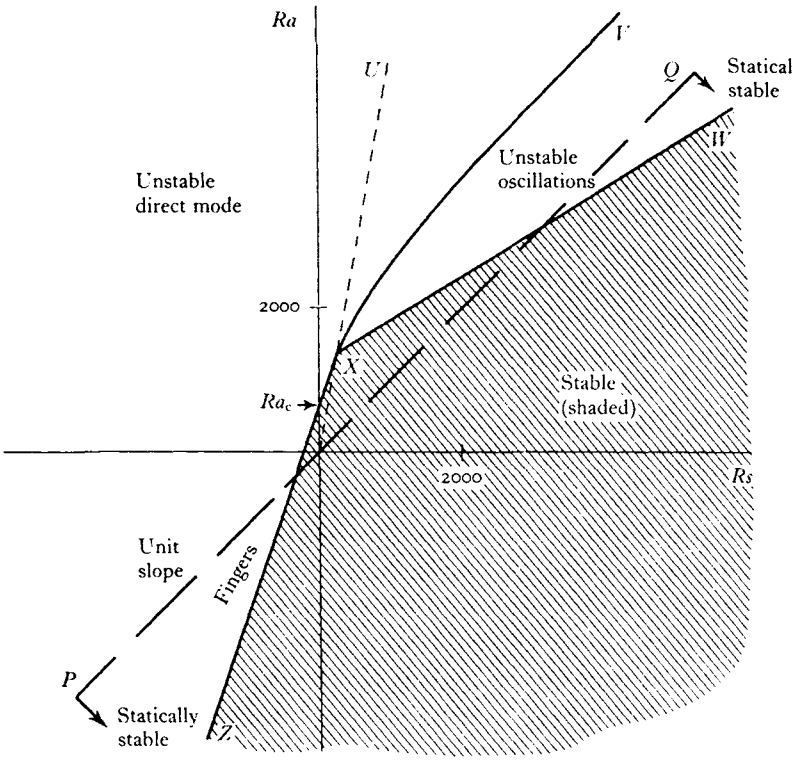

Fig. 8.2. Diagram of the various convection regimes described by (8.1.8). The sign convention is such that negative Ra and positive Rs represent stabilizing gradients of the respective components. (After Baines and Gill 1969.)

In the 'finger' regime (Ra and Rs both negative) instability sets in (when τ is small) at values of $|Rs|$ only slightly larger than the critical value for a salinity gradient alone, and certainly while the net density gradient is still statically stable (i.e. below the line PQ on which $Ra = Rs$). The motion just to the left of XZ is a direct, exponentially growing mode ($p_1 = 0$), drawing its potential energy from the component of lower diffusivity. For large negative values of both Ra and Rs, convection can occur only while $|Ra| < |Rs|/\tau$ or

$$\frac{\alpha \Delta T}{\beta \Delta S} < \frac{\kappa}{\kappa_S}, \tag{8.1.10}$$

which becomes an important consideration when the diffusivities are comparable.

Instability in the 'diffusive' regime (Ra and Rs both positive) occurs, as suggested by the above qualitative discussion, in an 'overstable' or oscillatory mode, since $p_1 \neq 0$ just above XW. When $\tau \ll 1$ the effective Rayleigh number may now be defined as $Ra_e = Ra - Pr \cdot Rs/(Pr+1)$ and the critical 'thermal' Rayleigh number is

$$Ra_c^0 = \frac{Pr}{1+Pr} Rs + \tfrac{27}{4}\pi^4. \tag{8.1.11}$$

For a given stable 'salt' gradient, Ra_c^0 must exceed the ordinary criterion by $Pr \cdot Rs/(1+Pr)$; in some problems (see §8.2.1), this correction can be so small as to be negligible, though the oscillatory mode of breakdown is preserved. When $Rs \gg \frac{27}{4}\pi^4$, the instability occurs when $Ra_c^0 \approx (Pr+\tau)Rs/(1+Pr)$, i.e. when the net density field is statically stable, since XW crosses PQ at some Rs. The frequency of the most unstable mode, when translated into the dimensional variables, is then

$$[(1-\tau)/3(Pr+1)]^{\frac{1}{2}}N; \tag{8.1.12}$$

this is always less than the buoyancy frequency, the factor being about $\frac{1}{3}$ for the case of heat and salt. Above the line XV the motion has a direct instead of an oscillatory form, if the limiting case $p_1 \to 0$ is also interpreted as steady convection. As $Rs \to \infty$, XV is parallel to PQ and the direct mode becomes possible just after the net density gradient becomes statically unstable (not only at the much larger Ra, above XU, as had previously been suggested).

8.1.3. *The form of the convection cells*

The analysis outlined above has been extended to calculate the growthrate of disturbances with any specified wavenumber. For given Ra and Rs (not just the critical values) one can determine the aspect ratio of the cells which will grow most rapidly. In spite of the limitations imposed by the linearized analysis, which is strictly valid only very close to the critical state, it appears that this gives some guidance as to what is in fact observed under highly supercritical conditions. (See §8.3.3.)

For all Ra, Rs the most unstable mode has $n = 1$, i.e. the cells extend from top to bottom of the unstable region. On the 'marginal' lines XZ and XW, $n = 1$ and $a^2 = \frac{1}{2}$ are the appropriate values (this most unstable horizontal wavenumber has already been taken into account in the numerical values quoted above). The behaviour of the maximum growthrate, and the value of a^2 at which this occurs for general Ra, Rs, were again given by Baines and Gill for the case $Pr = 10, \tau = 10^{-2}$. The line above which the most unstable mode is direct then lies just above XV in fig. 8.2, and is so close to it that where both modes are possible it is virtually certain that the motion will be direct. Through the whole top part of the diagram, where the difference in temperature (the property with the higher diffusivity) is driving the motion, the most unstable wavenumber is near unity; the cells are about as wide as they are high whether the motion is direct or oscillatory.

In the lower left-hand quadrant, however, maximum growth at supercritical $|Rs|$ (to the left of XZ) implies a relatively large a^2 so that cells tend to be tall and thin. Asymptotically, as $|Ra| \to \infty$ with $\tau \ll 1$, the wavenumber a_* of maximum growth is (in dimensional units)

$$\pi a_* \approx \left(\frac{g\alpha\Delta T/d}{\nu\kappa}\right)^{\frac{1}{4}}. \tag{8.1.13}$$

This result was obtained originally by Stern (1960) as the scale of the fastest growing disturbances of square planform but, as discussed in §7.1.2, linearized analysis can give no information about the actual structure in the horizontal. Although cells with $a \approx n$ are preferred just above the critical point, at large $|Ra|$ thin columns can evidently release the potential energy of the salt field more efficiently. This justifies the name given to the regime where Ra and Rs are both negative, and it is also in agreement with the observed form of 'salt fingers' in their fully developed state.

Note also that the form of (8.1.13) is the same as that derived in §7.4.2 for the thickness of a 'buoyancy layer' at the boundary of a fluid stratified with a single component (7.4.8). In both cases the basic gradient is statically stable, and it is the horizontal diffusion of this component which allows the fluid to react to an extra source of potential energy.

When τ is no longer very small (i.e. the diffusivities are comparable), another limiting case is of interest. As $|Ra| \to \infty$ with $Ra \sim Rs$ (nearly compensating density gradients), the predicted horizontal lengthscale in the finger regime is of the form (8.1.13), but with the net density gradient $\Delta\rho/\rho d = (\alpha\Delta T - \beta\Delta S)/d$ replacing $\alpha\Delta T/d$.

8.1.4. *Finite amplitude calculations*

Detailed calculations of the motions produced by finite amplitude disturbances of a double-diffusive system (starting with the same initial state considered in §8.1.2) were first made by Veronis (1965, 1968) and Sani (1965). Both these authors concentrated on the 'diffusive' regime (e.g. a stable salinity gradient, heated from below); and the description given here follows the most recent of these papers.

With the non-linear (product) terms added to (8.1.3) and (8.1.4) (cf. (7.2.2) and (7.2.3)), Veronis expanded ψ, T and S as double Fourier series in x and z (an extension of his method for a single component). Substituting in the governing equations and truncating after a finite number of terms (M in the horizontal and N in the vertical) gives a set of equations for the (time-dependent) coefficients. These can be solved numerically, taking into account all components and interactions such that $M+N \leqslant K$. The complexity increases rapidly with K, and Veronis treated $K = 4, 6, 8$ and 10. He regarded the answers as reliable when they changed little as K was increased, and showed that his earlier (1965) approximation with $K = 2$ was inadequate. The horizontal wavenumber was kept fixed throughout at $a^2 = \frac{1}{2}$ which is the most unstable value in the linear theory (cf. §7.1.2).

These calculations show that with $\tau = 10^{-\frac{1}{2}}$ and $Pr = 1$ and above, the onset of instability appears as an oscillatory mode at the $Ra = Ra_c{}^0$ predicted by linear theory (8.1.11). As Ra is further increased, a finite amplitude instability, leading to steady convection and an increased flux of T, sets in below the line XV (fig. 8.2). As $Rs \to \infty$, the criterion for this direct mode is again $Ra \to Rs$ (a marginally stable density gradient). When Pr is small, on the other hand, the first instability appears in the finite amplitude steady mode.

The main results of Veronis' analysis are the values of horizon-

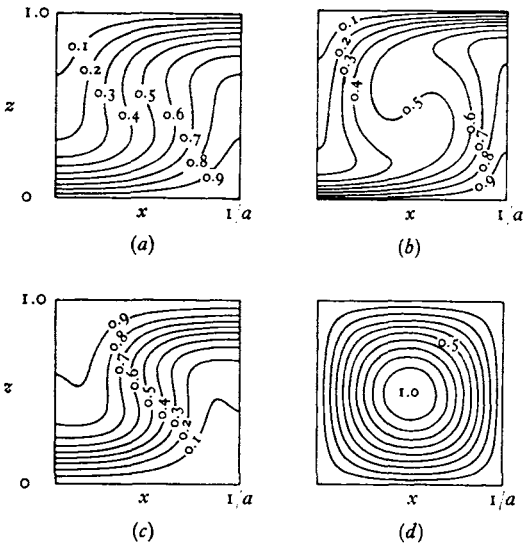

Fig. 8.3. Contours of (*a*) T, (*b*) S, (*c*) ρ and (*d*) ψ in a half cell, calculated by Veronis (1968) for the case $\tau = 10^{-\frac{1}{2}}$, $Pr = 1$, $Rs = 10^3$ and $Ra = 2500$. The lines $x = 0$ and $x = 1/a$ are lines of symmetry for T, S and ρ and lines of antisymmetry for ψ.

tally averaged T and S fluxes (F_T and F_S in density units), made non-dimensional with the molecular fluxes, i.e. the 'Nusselt numbers' Nu and Nu^s (see §7.1.1), which are functions of Ra, Rs, τ and Pr. A stabilizing gradient of solute inhibits the onset of convection and reduces the calculated F_T at moderate values of Ra. When Ra is sufficiently large, the strong finite amplitude (steady) motions which develop will tend to mix the solute so that the interior region is more nearly neutrally stratified; the fluid layer then transports nearly as much of the destabilizing T component as it does when this is present alone. Contours of T, S, ρ and ψ in a half cell show this tendency even at $Ra = 2500$ (fig. 8.3) and horizontal averages exhibit a slight reversal of the gradients in the central region.

Both F_T and F_S are increased by convection, and the ratio of these two fluxes is of special interest. In the limit $R_S \to \infty$, $Rs/Ra \to 1$, Veronis has shown that $F_T/F_S \to -\tau^{-\frac{1}{2}}$ (a result which will be derived in a more mechanistic way in §8.3.1). It also follows that

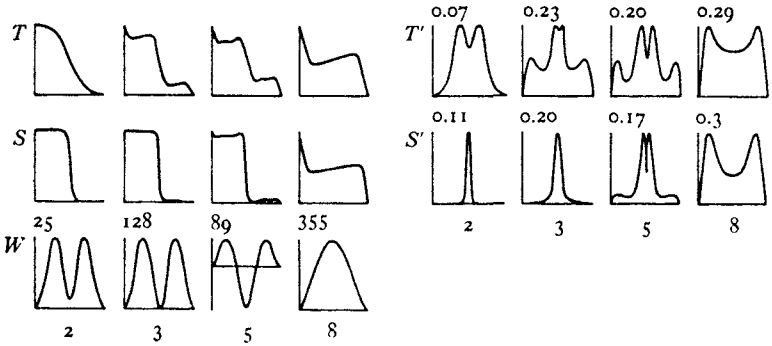

Fig. 8.4. The development of a T, S interface, as calculated by Elder (1969*b*). Mean values of T and S, the velocity W and fluctuations T' and S' are plotted at four times, with the height axis horizontal and the origin taken at the lower boundary. The parameters are $Ra = 10^6$, $Rs = 4 \times 10^6$, $\tau = 10^{-2}$ and the relative magnitudes of the peaks are marked.

the mean 'coefficient of diffusion for density' κ_ρ (defined as the ratio of the flux to the gradient) is in this limit.

$$\kappa_\rho \to -(\kappa\kappa_S)^{\frac{1}{2}}. \tag{8.1.14}$$

The negative sign reflects the fact that for energetic reasons F_T must always exceed F_S, and so the density flux is against the gradient.

In the case of the periodic oscillatory mode, calculations at finite amplitude show that the horizontally averaged density gradient changes sign at a particular height. For most of the cycle, and in the temporal mean, there is a stably stratified region near the boundaries and an unstable interior; but note that the overall density gradient is unstable, in contrast to the observed flows to be described later.

Elder (1969*b*) has used a 'mean field' approximation (cf. Herring 1964, and §7.2.3) to treat a double-diffusive problem with different and very revealing initial conditions. He started with a step (or sharp interface) between two well-mixed layers, each having the properties of the adjoining boundaries, with higher T and S below and a net stable stratification (again the 'diffusive' regime). The sequence of events is shown in fig. 8.4, where both mean and fluctuating properties are plotted. At first the interface thickens by diffusion, the T interface more rapidly than the S interface. The outer part thus becomes unstable, and fluctuations which were imposed initially begin to grow, with at first a weak oscillation appearing. Later there is a rapid exponential growth and break-

down, and the interface is sharpened by the increased mixing at its edges. During this period there is a balance between diffusion which tends to spread the interface, and mixing on either side which sharpens it – features which are also prominent in the laboratory experiments. The transfers across the interface produce two layers which for a time behave like isolated thermal layers, and the fluxes from the boundaries also become important. Eventually the interface is disrupted (by a mechanism which is not clear from the numerical experiment), and a single convecting layer is produced, with reversed gradients across the central layer.

8.2. The formation of layers; experiments and observations

We now turn to a discussion of laboratory experiments on double-diffusive systems, commenting at the same time on their relation to the predictions set out in §8.1, and adding some more theoretical ideas where appropriate.

8.2.1. *The 'diffusive' regime*

The simplest example of a 'diffusive' system (defined in §8.1.1 as one in which the energy to drive convective motions comes from the component T having the larger diffusivity) is a linear stable salinity gradient, initially at constant temperature and heated strongly from below. Convection is first observed in a layer close to the bottom, as the diffusion of heat makes the density gradient unstable there (cf. §7.3.1). The motions do not immediately extend through the whole depth of the fluid, however, as in ordinary thermal convection, and as predicted by the theories based on linear gradients of both properties. Instead, a series of convecting layers forms in succession, from the bottom up, as shown in fig. 8.5 pl. XIX. The salinity distribution maintains a stable density jump across each of the interfaces while the more rapid diffusion of heat relative to salt provides an unstable buoyancy flux which drives the convection. Each stage of this process will now be examined briefly in turn.

Shirtcliffe (1967, 1969*a*) has shown that the initial instability does occur as a growing oscillation, as predicted by theory. (See fig. 8.6.) He obtained fair quantitative agreement with both the

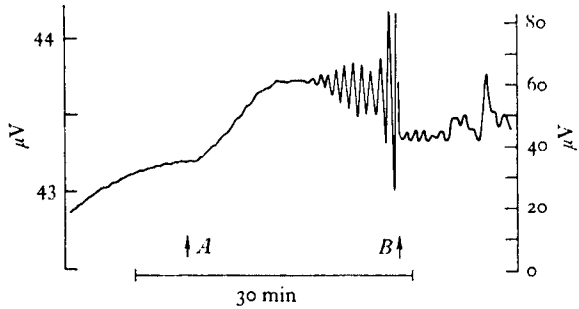

Fig. 8.6. Section of a differential thermocouple record obtained by Shirtcliffe (1967), *Nature*, **213**, 489–90, showing the overstable breakdown of a stratified sugar solution heated from below. The heating rate was changed at '*A* and the right-hand voltage scale applies after *B*.

critical Rayleigh number criterion (8.1.11) and the frequency (8.1.12), provided the depth of the layer is defined as that which makes the effective Rayleigh number a maximum. Allowance for the non-ideal boundary conditions (Nield 1967) improves the agreement between theory and experiment. Only a very small stabilizing gradient is needed to produce the overstable mode of breakdown (see fig. 8.2). For example, Hurle and Jakeman (1971) have shown that the Soret effect (i.e. mass diffusion caused by a temperature gradient) can produce concentration gradients near a boundary which are sufficiently large for this purpose, even in extremely dilute solutions. They have documented this phenomenon with experiments in water–methanol mixtures, and have also suggested it as an explanation of temperature oscillation and impurity striations observed during the growth of crystals from liquid metals.

As heating is continued beyond the point of instability, a well-mixed layer develops; this behaviour too is consistent with the finite amplitude calculations leading to fig. 8.3. The top of the layer is rising, however, as fluid from the gradient region above is incorporated into it, and its growth can be calculated as follows. Assuming a constant heat flux H and a linear initial gradient of solute denoted by $N_S^2 = -g\beta\,\mathrm{d}S/\mathrm{d}z$, the heat and solute balances in a uniformly mixed layer with depth d at time t give

$$\left.\begin{aligned} Ht &= -\rho C\, d\Delta T, \\ \text{and} \qquad g\beta\Delta S &= \tfrac{1}{2} d N_S^2, \end{aligned}\right\} \tag{8.2.1}$$

where T and S are the steps of 'temperature' and 'salinity' at the top of the layer, C is the specific heat, and the rest of the notation is that used in §8.1.2.

Experimentally it is observed that

$$\alpha\Delta T = -\beta\Delta S, \tag{8.2.2}$$

i.e. the steps in T and S are compensating to within the experimental error, and the net density structure is as shown in fig. 8.7*b* (compare with §7.3.4, where an experiment using heat alone is described). Combining (8.2.1) and (8.2.2), and using the buoyancy flux $B = g\alpha H/\rho C$ defined in (5.1.7), we obtain

$$d = 2^{\frac{1}{2}} B^{\frac{1}{2}} N_S^{-1} t^{\frac{1}{2}} \tag{8.2.3}$$

and

$$g\alpha\Delta T = -g\beta\Delta S = 2^{-\frac{1}{2}} B^{\frac{1}{2}} N_S t^{\frac{1}{2}}. \tag{8.2.4}$$

If, on the other hand, a fixed fraction of the kinetic energy generated by buoyancy in the unstable layer were used to mix fluid across the interface, d and ΔS would be increased above the values just calculated, though the form of the relations remains the same. (This possibility could become relevant on a larger scale, and will be referred to again in chapter 9.) In the limit where the energy is conserved between the initial and final states, (8.2.2) is replaced by $\alpha\Delta T = -\frac{1}{3}\beta\Delta S$ and the distribution of properties is as shown in fig. 8.7*a*. There is now a definite density step at the top of the layer; d is increased and ΔT is decreased by a factor of $\sqrt{3}$ compared to (8.2.3) and (8.2.4).

The relations (8.2.3) and (8.2.4) have been verified directly over a range of strong heating rates by measuring the depth and temperature of the growing convecting layer (Turner 1968*a*). (Rather better agreement with experiment is obtained by taking into account the diffusive boundary layer ahead of the convecting zone; this will be invoked explicitly below.) At some point the growth stops abruptly; a second layer forms on top of the first and behaves in the same way, until the many layers illustrated in fig. 8.5 have built up. (Note that sidewall heating can lead to a similar effect, which will be discussed separately in §8.2.3.) A purely vertical heat flux produces layer depths which depend on the initial gradient and heating rate, and the measured thickness of the first layer at the time a second forms above it can be explained as follows.

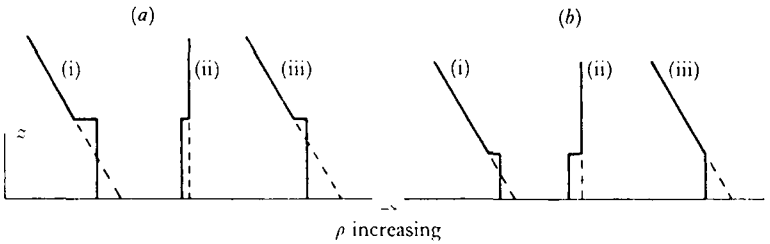

Fig. 8.7. The distributions of (i) density due to salinity, (ii) density due to temperature, and (iii) the net density produced by heating a linear salt gradient from below. It has been assumed that (*a*) all the potential energy released by heating is used to redistribute salt, and (*b*) the top of the mixed layer is marginally stable. (From Turner 1968*a*.)

The diffusive thermal boundary layer growing ahead of the well-mixed layer has thickness $\delta \propto t^{\frac{1}{2}}$, and is thus a constant fraction of the layer depth d which can be written as

$$\delta/d = 2\kappa N_S^2/B. \tag{8.2.5}$$

When δ/d is small (i.e. B is sufficiently large), Rs based on δ and N_S^2 is much less than Ra based on δ and ΔT, so the criterion for instability (8.1.11) is effectively a condition on Ra alone. Instability occurs when the depth d is

$$d_c = \left(\frac{\nu Ra_c}{4\kappa^2}\right)^{\frac{1}{4}} B^{\frac{3}{4}} N_S^{-2} \tag{8.2.6}$$

or when ΔT (proportional to dN_S^2) reaches a corresponding value determined only by B. The form of (8.2.6) has been verified experimentally, though the implied numerical value of Ra_c is larger than the application of the simplest theory would suggest. The corresponding calculations for later layers would have to allow for the dependence of the fluxes through the first interface on the changing S and T differences across it (see §8.3.1).

Shirtcliffe (1969*b*) has used another approach to explain his laboratory observations of successive layering in the limit where δ/d is not small. He modelled the process numerically, using diffusion coefficients which changed abruptly from molecular to much larger 'eddy' values when a Rayleigh number criterion for instability was exceeded locally. The observed features of successive layer formation at the top, and the merging of previously formed

layers at the bottom when their densities become equal (see fig. 8.5) are reproduced well, but of course many detailed questions about the mechanism of transfer through the various regions are left unanswered.

8.2.2. *The 'finger' regime*

In the opposite case to that described above, when a little hot salty water is poured on top of a stable temperature gradient, 'salt fingers' very quickly form, as predicted by the first of the stability criteria (8.1.9). A cross section of these long narrow convection cells, made visible by adding fluorescent dye at the bottom, is reproduced in fig. 8.8 pl. xx. (Later it will be shown that the planform in the idealized case is square, with upward and downward motions alternating in a close packed array. Practically, this means that each 'finger' tends to have four near neighbours, though their orientation may gradually change. See fig. 8.18 pl. xxi.)

This process looks very different from that illustrated in fig. 8.5, for example, but consider the results of another related series of experiments. If a layer of lighter sugar solution (the more slowly diffusing component, denoted by S in the notation of §8.1.2) is placed above a stable gradient of salt (T), the configuration again gives rise to 'fingers', since the substance of lower diffusivity is again unstably stratified, though τ is about $\frac{1}{3}$ instead of 10^{-2} for heat and salt. These solutes are very convenient to use in the laboratory, since they allow large gradients to be set up without requiring any special precautions to prevent losses at the boundaries. When the salinity gradient is large in relation to the concentration step, fingers develop and eventually extend right to the bottom of the container (as in the experiment with heat and salt shown in fig. 8.8). With a rather smaller T gradient and the same step of S at the top, however, a convecting layer is formed; the fingers become unstable and overturn over a finite depth. The layer deepens, bounded by a sharp interface below which fingers persist. These in turn can become unstable, leading to a second convecting layer separated from the first by an interface containing fingers. In time, a series of such convecting layers can be formed, as shown in fig. 8.9 pl. xx.

Looked at in the large, therefore, and ignoring for the present the details of interface structure and the differences in the mechanism of

transport which will be taken up in §8.3, there is a complete correspondence between the 'finger' and 'diffusive' systems. The inequality of molecular diffusivities results in an unstable buoyancy flux across a statically stable interface in both cases, and this maintains the convection in the layers above and below. In the 'finger' system this buoyancy flux is dominated by the S component, and hence such interfaces must reverse the relative rates of transport due to molecular processes alone (e.g. salt is transported faster than heat across an interface containing fingers).

A theory of layer formation in this case has been proposed by Stern and Turner (1969) along similar lines to that outlined previously, but now taking more explicitly into account the 'finger' structure of the interface. The criterion for instability of a deep layer containing fingers must also be taken into account here (see §8.3.4).

8.2.3. *Side boundaries and horizontal gradients*

It was remarked in §8.2.1 that laboratory experiments on the formation of layers by heating a salt gradient from below can be complicated by heating or cooling from the side walls. Though vertical transfer processes are always important once layers have formed, their depth can be set by these side wall effects, rather than by the criterion (8.2.6). The mechanism is readily understood (qualitatively at least) by extending the arguments of §7.4.2. There we saw that a distortion of the interior distribution of a single component can produce a steady flow along a boundary, in which a constant difference of (say) temperature is maintained between the boundary layer and interior. If a stabilizing salt gradient is distorted by heating, however, such a balance cannot be maintained; two different boundary layer length scales become relevant and there is no velocity profile which can balance both T and S.

The formation and growth of layers in a two-component system is an unsteady process, which is related to the instability of the sidewall thermal boundary layer as it grows by conduction (cf. §7.3.1). When instability sets in, salt is lifted by the heated wall layer, but only to a level where the net density is close to that in the interior. Fluid then flows out away from the wall, producing a series of layers

which form simultaneously at all levels and grow inwards from the boundaries. This is shown beautifully in the experiments of Thorpe, Hutt and Soulsby (1969); it is clear from fig. 8.10 pl. xx, that each layer (marked by dye) then slopes downwards as it extends and cools. Chen, Briggs and Wirtz (1971) have shown that the layer thickness (when τ is small) is close to the natural lengthscale

$$l \approx \frac{\alpha \Delta T}{\beta \, \mathrm{d}S/\mathrm{d}z} \tag{8.2.7}$$

(where ΔT is the imposed horizontal temperature difference), which is the height to which a heated fluid element would rise in the initial density gradient.

Analogous effects can be obtained using two solutes instead of salt and heat. If opposing gradients are set up, the surfaces of constant concentration are horizontal and so the no-flux boundary conditions are satisfied for both properties on vertical walls. Such distributions can be very stable in the laboratory, a considerable finite amplitude disturbance being required to initiate layered convection in the interior. At an inclined boundary, however, density anomalies are produced by diffusion which tend to drive a flow along the wall. Again the second component prevents this continuing indefinitely, and fluid spreads into the interior as a series of layers.

The observed motions are much stronger than with a single solute and have some surprising features. Fig. 8.11 pl. xix shows an experiment started with linear gradients of salt overlying sugar. Just above the boundary is a downflow (as one might expect from the distortion of the thicker salinity boundary layer) but above this is an upslope counterflow. As the fluid moves outwards into the layers the vertical gradients are reversed locally and fingers form, though the original distribution was in the 'diffusive' sense. At a much later stage, a series of sharp diffusive interfaces remained, with flow down the boundary dominating. This produced a mean circulation which caused the layers to spread far from the boundary at the bottom and suppressed their extension near the top of the slope. (Under a sloping lid, the motions are reversed.)

The theoretical stability problem corresponding to these observations has not been solved (it is analogous to the Bénard problem

with large gap widths) but Thorpe, Hutt and Soulsby (1969) have analysed the simpler case of a fluid contained in a narrow slot. They assumed linear gradients of S and T initially in both the vertical and horizontal directions, with a statically stable (or zero) density gradient in the vertical and exactly compensating horizontal gradients. The stability condition can be expressed as a relation between two effective Rayleigh numbers defined as in §8.1.2., Ra_z being based on the vertical differences and Ra_x on horizontal differences of the two properties over a distance d, the separation of the plates. Asymptotically, at large Ra_z, the stability criterion for vertical walls is

$$|Ra_x|_{\min} = 2.76|Ra_z|^{\frac{5}{8}}, \tag{8.2.8}$$

so a minimum horizontal gradient is necessary for instability. Linear theory predicts that a steady motion will then be set up, with cells reaching right across the gap and having a height $d(2/|Ra_z|)^{\frac{1}{8}}$. A definite slope of the cell boundaries can also be calculated.

These relations were shown to be consistent with laboratory measurements carried out using a salinity gradient contained in a vertical slot 6 mm wide, with one wall heated slowly. Rather better agreement with these same experiments was obtained in a subsequent theory by Hart (1971*b*), who took into account the mean flow due to the sidewall heating at finite values of Ra_z, and also used more realistic boundary conditions. The observed motions in all cells do, however, differ from the predictions in one respect; they have the same sense of rotation (dominated by the flow up the hot wall and down the cold) instead of being counter-rotating in alternate cells as the theory suggested. More detailed observations of the motion and the temperature and salinity structure in a wider tank showed reversals of the gradients which are consistent with the same circulation pattern.

Horizontal gradients in the *interior* of a fluid can also lead to instabilities and the release of energy which produces a layered structure, without the need for disturbances propagating in from boundaries. Some of the essential physical features are illustrated by experiments which are a variation on the 'lock exchange' problem considered in §3.2.4. When one half of a channel is filled with hot salty water and the other with cold fresh water of the

same density, and a vertical barrier separating them is withdrawn, horizontal diffusion gives rise to vertical motions near the interface. A small initial tilt in either direction, introduced by removing the barrier, will grow and lead to the formation of two layers, stratified either in the 'diffusive' or 'finger' sense. In both cases vertical transports will increase the density difference between the layers (see §8.3), so reinforcing the original (fortuitous) direction of motion. In a deep fluid it seems likely that a preferred vertical scale which depends on both the vertical and horizontal gradients of the two properties should emerge from a stability argument.

8.2.4. *Related observations in the ocean*

Various observations in nature, and especially in the ocean, can be interpreted as examples of the phenomena discussed above. With this background we can now describe, more concisely and with better physical understanding, some of the most striking examples. Of course not all layered structures are the result of double-diffusive processes, and other mechanisms of layer formation will be discussed in chapter 10. The examples given here are distinguished fundamentally by the existence of opposing vertical gradients of temperature and salinity. In the observations so far ascribed to double-diffusive convection there is also a notable regularity and persistence of the steps, though the process could also be important under transient conditions which are not so easily recognized.

There are many fresh water lakes which have become stably stratified with salt, for example by an intrusion of sea water at some time in the past. Some of these are observed to be hotter at the bottom than the top, and well-mixed layers separated by 'diffusive' interfaces are formed. An especially well-documented example is Lake Vanda in Antarctica, studied by Hoare (1966), among others. Well-mixed layers of several scales are recorded, those nearest the surface being about $1\frac{1}{2}$ m deep, with the sharpest temperature transitions about 1 °C in 1 cm.

Steps maintained by cooling a salinity gradient from above, underneath an ice island in the Arctic ocean, are shown in the record of fig. 8.12, obtained by Neal, Neshyba and Denner (1969). Here the temperature steps are only a few hundredths of a °C, but they are

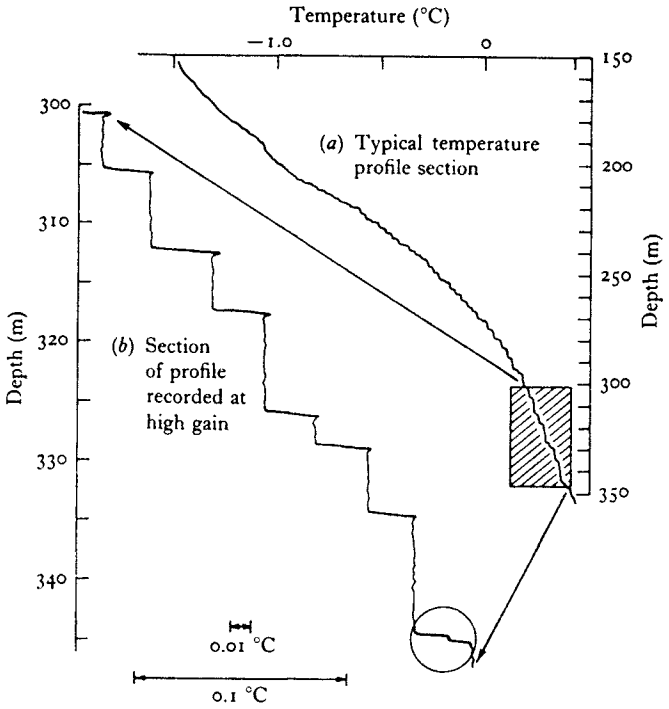

Fig. 8.12. Temperature profile under Arctic Ice Island T3, showing steps formed by the double-diffusive mechanism. (From Neal, Neshyba and Denner (1969), *Science*, **166**, 373–4. © 1969 by the American Association for the Advancement of Science.)

extremely regular, indicating (according to the results of §8.3.1) that the heat and salt fluxes must be uniform with depth. At the other extreme is the hot salty water found at the bottom of the Red Sea (Degens and Ross 1969). Two well-mixed layers have been observed, the bottom one nearly saturated and at about 56 °C, and the other at 44 °C and intermediate in salinity between this and the overlying water. The interface between them is so sharp that no sample has been obtained from it, and this too can be interpreted as a 'diffusive' interface separating two strongly convecting layers.

Good examples of layering consistent with the 'finger' process have also been found by many oceanographers, using continuously recording temperature–salinity–depth devices. Fig. 8.13 shows a series of layers about 20 m thick, recorded by Tait and Howe (1968,

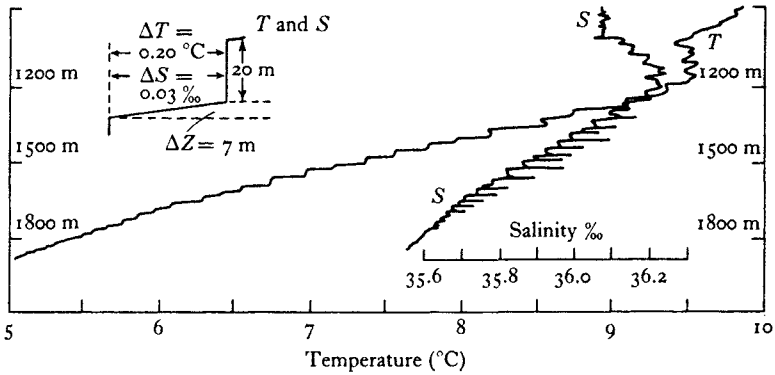

Fig. 8.13. A series of layers in T and S observed under the Mediterranean ouflow into the Atlantic, and attributed to the 'finger' mechanism. The sharp spikes to the right of the salinity trace are instrumental and can be ignored. The inset summarizes the mean properties of the layers and interfaces. (From Tait and Howe (1971), *Nature*, **231**, 178–9.)

1971) deep in the Atlantic underneath the Mediterranean outflow, where warm salty water overlies colder fresher water. Such layers have been observed relatively rarely, though the mean distributions of temperature and salinity appear to favour their formation elsewhere as well. The results discussed in §8.3.4 suggest that externally generated turbulence may be responsible for inhibiting the formation of fingers. No observations of the 'fingers' themselves have been made in the ocean, though of course such a direct measurement would greatly increase our confidence in the double-diffusive explanation of this regular layering.

It is worth pointing out that conditions are particularly favourable for double-diffusive convection when a layer with compensating temperature and salinity differences intrudes into an environment with different properties (as the Mediterranean outflow does). This guarantees that the net density difference will be small, and it is shown in the following section that the fluxes will then have their maximum values. Another example of this effect has arisen in the context of sewage disposal in the sea off California (Fischer 1971). Effluent, which can be regarded as nearly fresh water, flows out of a pipe laid along the bottom and rises as a line plume. The sea in this area is strongly stratified in temperature, and so the effluent, diluted with cold sea water, spreads out in a layer below the thermo-

cline (see §6.4.2). This layer, however, remains colder and fresher than the water above it, and the salt finger mechanism can cause it to thicken and even extend to the surface.

The importance of boundary processes is brought out by observations of layers formed in the main thermocline near Bermuda (where the stratification is in the 'finger' sense) (see Wunsch 1970). The stepped structure is much clearer near the slope than few miles from it, but the validity of applying the laboratory results of §8.2.3 here is rather doubtful. It seems likely that layers form not as a result of a diffusive instability but directly because of turbulent mixing near the slope (as described in §4.3.4). However they are formed initially, such layers will be mixed and the interfaces kept sharp by the buoyancy flux carried by the salt fingers.

Layering and fine structure associated with horizontal gradients of T and S has also been reported. For example, Stommel and Fedorov (1967) were able to trace layers several kilometres horizontally, and to show that the density in them remained constant (to the accuracy of measurement) while T and S both varied in a compensating manner. Pingree (1971) has demonstrated the importance of horizontal variations, in his discussion of the less regular small scale structures above and below the Mediterranean outflow. The T and S fluctuations are highly correlated and compensating in density (whatever the signs of the mean gradients); this observation cannot be explained in terms of vertical mixing alone, but requires some horizontal advection or vertical shear. The regular layering described previously may, on the other hand, be favoured in more uniform regions where the horizontal motions are weak (see Zenk 1970).

8.3. The fluxes across an interface

Once layers and interfaces have formed in one of the ways described, the most important property is the flux of S and T across them. In this section we discuss laboratory measurements of these fluxes, and more detailed observations aimed at relating them to the structure of the interface. Ideally one would like to examine a number of identical layers in a steady state, but so far only quasi-steady two-layer systems have been used, with a single interface and solid boundaries (or a free surface) above and below. The 'diffusive'

systems will be discussed first, but many of the ideas carry over to the 'finger' case.

8.3.1. *Measurements in the 'diffusive' regime*

The overall behaviour of a two-layer convecting system, with a hot salty layer below cold fresh water for example, can be interpreted using an extension of the earlier dimensional arguments, which led to (7.1.9) and (7.1.10) in the case of high Rayleigh number single component convection. The flux of the driving component F_T across a convecting layer of depth d, and therefore through the bounding interfaces in a steady state, must now be of the form

$$Nu = f(Ra, Rs, Pr, \tau), \tag{8.3.1}$$

where $$Nu = \frac{F_T}{\kappa \Delta T/d}, \quad Ra = \frac{g\alpha \Delta T d^3}{\nu\kappa}, \quad Rs = \frac{g\beta \Delta S d^3}{\nu\kappa}$$

as defined in §8.1.2, and $Pr = \nu/\kappa$, $\tau = \kappa_S/\kappa$. ΔT and ΔS are the T and S differences 'across a layer', or by symmetry in the ideal situation, between the centre of one layer and the centre of the next.

In any experiment $\beta\Delta S/\alpha\Delta T = Rs/Ra$ is given and Pr and τ are constants, and a plausible form of (8.3.1) which removes the dependence on d is

$$Nu = f_1\left(\frac{\beta\Delta S}{\alpha\Delta T}\right) Ra^{\frac{1}{3}}. \tag{8.3.2}$$

Note that the choice of Ra as the major parameter in (8.3.2) is to some extent arbitrary; a more general combination of Ra and Rs (such as the effective Rayleigh number used in §8.1.2) would also be consistent with (8.3.1). Equation (8.3.2) is equivalent to (cf. (7.1.10))

$$\alpha F_T = A_1(\alpha\Delta T)^{\frac{4}{3}}, \tag{8.3.3}$$

where A_1 has the dimensions of velocity. It is to be understood that f_1 and A_1 can depend on molecular properties but once the two components are specified, they should be functions only of the density ratio $R_\rho = \beta\Delta S/\alpha\Delta T$.

The deviations of A_1 from the value A obtained for solid boundaries with only a difference ΔT between them are a measure of the effect of an increasing ΔS on F_T. Measurements by Turner (1965) in the heat–salt system, which were compared with the 'solid plane'

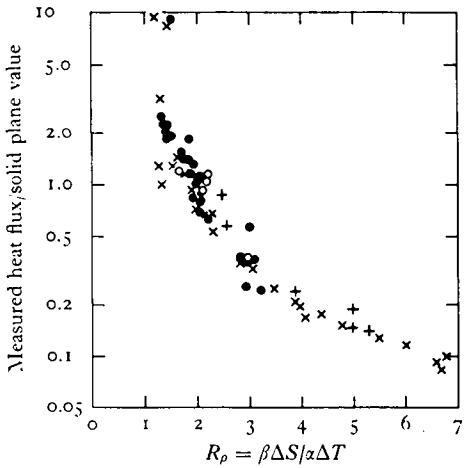

Fig. 8.14. The measured heat flux across the interface between a hot salty layer below a cooler fresher layer, compared with the value calculated for solid plane boundaries. This ratio has been plotted against the density ratio R_ρ; the different symbols refer to experiments with different heating rates at the lower boundary. The three points at the top of the figure are now judged to be unreliable. (From Turner 1965.)

values in this way, are shown in fig. 8.14. They confirm that the ratio A_1/A can indeed be expressed as a function of R_ρ alone. For $R_\rho < 2$, the heat flux is greater than it would be above a solid plane (i.e. if a thin conducting foil were inserted at the centre of the interface). This increase can be associated with two effects: the interface behaves more like a free surface, so that there is a weaker constraint on the horizontal motion, and it also supports waves which can break, so increasing the effective surface area. When $R_\rho > 2$ the heat flux falls progressively below the solid plane value as R_ρ is increased, reaching about a tenth of that value when $R_\rho = 7$. Huppert (1971) has suggested that over the whole of the measured range, the empirical functional form

$$A_1/A = 3.8(\beta\Delta S/\alpha\Delta T)^{-2} \tag{8.3.4}$$

fits the observations to the experimental accuracy.

Similar arguments can be used to express the salt flux as a function of Ra and $R_\rho = \beta\Delta S/\alpha\Delta T$, which will have a form like (8.3.2) independent of d. It follows that the ratio of the fluxes, expressed in

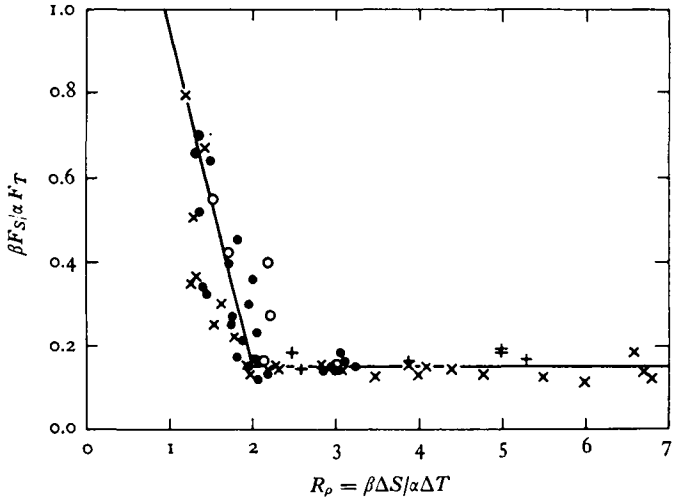

Fig. 8.15. The ratio of the potential energy changes due to the transfer of salt and heat across an interface between a hot salty layer below a cooler fresher layer, plotted as a function of the density ratio R_ρ. (From Turner 1965.)

terms of their respective contributions to the density (or potential energy) flux will be

$$\beta F_S/\alpha F_T = f_*(\beta\Delta S/\alpha\Delta T). \tag{8.3.5}$$

For given molecular properties, the flux ratio should be another systematic function of R_ρ, and this is again borne out experimentally as shown in fig. 8.15. As $R_\rho \to 1$, $\beta F_S/\alpha F_T \to 1$ also, suggesting (in agreement with our interpretation of the increased heat flux in this range) that heat and salt are here being transported by the same turbulent motions at a breaking interface. As R_ρ increases to 2, the flux ratio falls rapidly, since molecular processes become increasingly important. The most striking feature of the results is that for $R_\rho > 2$ the flux ratio remains constant to within the experimental error, the mean value for salt and heat being $\beta F_S/\alpha F_T = 0.15$. Note that when these results are combined with (8.3.4) they imply that the maximum net density flux for a given ΔT occurs at $R_\rho = 2$.

Shirtcliffe (personal communication) has carried out the corresponding measurements for a diffusive interface between two concentrated solutions at the same temperature (salt above sugar). These confirm the constancy of $\beta F_S/\alpha F_T$ over a range of R_ρ, his

measured value for NaCl and sucrose being 0.60 ± 0.02. Using an elegant optical technique, he also deduced profiles of the two components through the interface. He showed that the fluxes of each of them in his experiment could be explained completely by ordinary molecular diffusion through the measured gradients (using diffusion coefficients corrected for the presence of the other property). This deduction makes the name 'diffusive interface' a particularly suitable and descriptive one.

There is as yet no completely satisfactory theory which reconciles these last two results, though it is clear from both the laboratory and numerical experiments that the adjustment between the stable, diffusing interface and convecting layers must take place in a thin boundary layer separating them. A simple model of this layer has been proposed by Rooth (quoted by Veronis (1968)), which has features in common with that of Howard (1964) for a single component (see §7.3.1). Starting with sharp steps of both properties ($(\Delta T)_*$ and $(\Delta S)_*$ say), T and S boundary layers will grow by diffusion to thicknesses proportional to $\kappa^{\frac{1}{2}}$ and $\kappa_S^{\frac{1}{2}}$. If these are swept away intermittently by the large scale convecting motions, then the ratio of the amounts of buoyancy removed (i.e. the ratio of the fluxes) will be

$$\frac{\beta F_S}{\alpha F_T} = -\frac{\beta(\Delta S)_*}{\alpha(\Delta T)_*}\tau^{\frac{1}{2}}. \tag{8.3.6}$$

Under the conditions envisaged in Veronis' calculation (§8.1.4), $\alpha(\Delta T)_*$ and $\beta(\Delta S)_*$ are the whole differences $\alpha\Delta T$ and $\beta\Delta S$ imposed at the boundaries and are equal when $Rs/Ra \to 1$; it follows that $\beta F_S/\alpha F_T \to -\tau^{\frac{1}{2}}$ in that case. The same argument will apply when the differences are unequal, provided one adds the assumption that only the statically unstable edge of a diffusive interface will be swept away, i.e. down to the level where $\alpha(\Delta T)_* = \beta(\Delta S)_*$, even when $\beta\Delta S > \alpha\Delta T$. The constancy of the flux ratio certainly implies that there is some kind of self-limiting mechanism which makes the convecting layers insensitive to the total differences.

The measured flux ratios for salt–heat and sugar–salt are roughly in agreement with this prediction, though the correspondence is not exact and the details of the balance mechanism are probably more complicated. Corresponding measurements have also been made

using layers containing several solutes S_x with different molecular diffusivities κ_x, which are driven across an interface by convection induced by heating from below. Turner, Shirtcliffe and Brewer (1970) have shown that the individual 'eddy transport coefficients' (defined as the flux divided by the mean gradient) are different, and approximately proportional to $\kappa_x^{\frac{1}{2}}$. This is consistent with (8.3.6) only if $(\Delta S)_*$ for each stabilizing component is proportional to the *whole* difference of each property across the interface; this result too awaits a detailed theoretical explanation.

Linden (1971*b*) has given a mechanistic argument which puts some numbers into the explanation of the increase in the flux ratio at lower values of R_ρ. As the density ratio is reduced, the direct entrainment of both properties across the interface becomes increasingly important relative to the intermittent breakdown mechanism. The buoyancy flux through the interface can be used to estimate the turbulent velocities in the layers (cf. § 5.1.3), which are then related to the entrainment through the results of the mechanical stirring experiments described in § 9.1.

8.3.2. *The time-history of several convecting layers*

Using experimental data for the two fluxes across an interface (such as those summarized in figs. 8.14 and 8.15 for a 'diffusive' salt–heat system), it is straightforward to calculate the changes with time of T and S in the individual layers. Consider first the simplest case of two layers, the upper depth d_1 and the lower of depth d_2, convecting at high Rayleigh number because of a double-diffusive flux across the bounding interface and with impermeable top and bottom boundaries. The fluxes are given in terms of either the rate of change of properties or the differences between the layers by

$$\left.\begin{aligned} \alpha F_T &= d_1 \alpha \frac{\mathrm{d}T_1}{\mathrm{d}t} = -d_2 \alpha \frac{\mathrm{d}T_2}{\mathrm{d}t} = A_1(\alpha \Delta T)^{\frac{4}{3}}, \\ \text{and} \qquad \beta F_S &= d_1 \beta \frac{\mathrm{d}S_1}{\mathrm{d}t} = -d_2 \beta \frac{\mathrm{d}S_2}{\mathrm{d}t} = f_* \alpha F_T, \end{aligned}\right\} \tag{8.3.7}$$

where A_1 and f_* are functions of $(\beta \Delta S/\alpha \Delta T)$, which are in principle known. Rearrangement gives two equations for ΔT and ΔS, from which T_1, S_1 and T_2, S_2 can be deduced as functions of time.

Because the driving energy comes from the T distribution, f_* must be less than one, and the net density difference $\Delta\rho/\rho = \beta\Delta S - \alpha\Delta T$ will *always* be increasing with time. When f_* is small the density difference increases most rapidly, since $\beta\Delta S$ remains little changed while the destabilizing $\alpha\Delta T$ is decreasing. As f_* approaches unity, the two fluxes are more nearly compensating, and there will be only a small change in $\Delta\rho$, but always in the stable sense. Both transports will fall to zero as $\Delta T \to 0$, i.e. when the driving component is nearly uniformly distributed in the vertical, but in this 'final state' $\Delta\rho/\rho = \beta\Delta S$ is non-zero and stable.

These points may seem obvious, but confusion can arise in defining the 'state of no motion' if they are not properly appreciated, and a closely related problem has led to a controversy in the astrophysical literature. Some large stars have a helium-rich core, which is heated from below and therefore convecting. Outside this core, lighter hydrogen predominates, but helium can be transported upwards by the convective stirring. Spiegel (1969) has pointed out that this is also a double-diffusive system, with the abundance of helium replacing salinity as the property of lower κ. The basic assumption used in computing some stellar models is that the convection outside the core can regulate itself to remain in a state of near convective neutrality, a process which has been called 'semi-convection'. From the arguments given above, it is clear that the criterion for convective neutrality must be that of uniform (potential) temperature, i.e. uniformity of the *driving* component, as assumed by Schwarzschild and Härm (1958). Uniform potential density is not the right assumption, since motions can persist when this increases with depth and appears hydrostatically stable.

The behaviour of a three-layer system, consisting of two effectively infinite layers between which ΔT and ΔS are specified (and unchanging) and which are separated by a finite layer with intermediate properties, has been investigated by Huppert (1971). He has proved that when $f_*(\alpha\Delta T/\beta\Delta S)$ is constant (e.g. when $R_\rho > 2$ in the heat–salt experiments), there is a range of combinations of

$$T = \tfrac{1}{2}\Delta T(1+\theta) \quad \text{and} \quad S = \tfrac{1}{2}\Delta S(1+\sigma)$$

of the middle layer which are in stable equilibrium. That is, under these conditions the fluxes of both properties across the two inter-

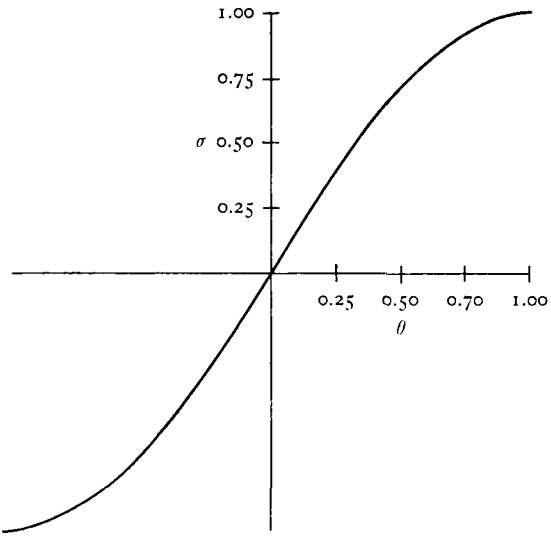

Fig. 8.16. The possible equilibrium states of an intermediate layer of temperature $T = \frac{1}{2}\Delta T(1+\theta)$ and salinity $S = \frac{1}{2}\Delta S(1+\sigma)$ lying between two semi-infinite layers whose properties differ by ΔT and ΔS. Note that the same steady fluxes of heat and salt can be maintained across the upper and lower interfaces even when the temperature and salinity steps are unequal. (From Huppert 1971.)

faces are equal, and layers started with other values of T and S will tend towards some point on the equilibrium curve. When f_* is not constant, the only equilibrium point occurs when T and S are at the mean values of the deep layers; even this is unstable, and the central layer will in time approach the density of one of the others and merge with it. Detailed results have been obtained for heat–salt diffusive interfaces in this geometry, and fig. 8.16 shows the 'equilibrium' curve calculated using the data from figs. 8.14 and 8.15. These results can be immediately generalized to apply to any number of interfaces and layers.

8.3.3. *Fluxes and structure at a 'finger' interface*

Because of the symmetry between the two systems remarked on in §8.2.2, many of the overall properties of a 'finger' interface can be described using a minor modification of the dimensional argument outlined in §8.3.1 for the diffusive interface. It seems logical (but

not essential) to emphasize still the difference in the driving component across the interface (now ΔS), so that (8.3.3) is replaced by

$$\beta F_S = A_2(\beta\Delta S)^{\frac{4}{3}}. \tag{8.3.8}$$

Again the factor A_2 depends on molecular properties, but when these are given, it is a function of the density ratio $R_\rho{}^* = \alpha\Delta T/\beta\Delta S$ (which is written here in the inverse sense so that again $R_\rho{}^* > 1$ denotes static stability). This form again receives support from laboratory experiments (Turner 1967). In the heat–salt system, the factor A_2 ($\approx 10^{-1}$ cm/s) is, however, about fifty times as large at $\alpha\Delta T \approx \beta\Delta S$ as it would be if the same constant salinity difference were maintained between solid boundaries; A_2 falls with increasing $R_\rho{}^*$ but is still about fifteen times this value at $R_\rho{}^* = 10$. A 'finger' interface is a much more efficient means of injecting a salt flux into a convecting layer than is pure diffusion.

The ratio of the fluxes can be expressed in the same way (cf. (8.3.5)) as

$$\alpha F_T/\beta F_S = f_*(\alpha\Delta T/\beta\Delta S). \tag{8.3.9}$$

Experimentally, f_* has again been shown to be constant over a wide range of $R_\rho{}^*$. Turner (1967) obtained the value $\alpha F_T/\beta F_S = 0.56$ for heat–salt fingers over the range $2 < R_\rho{}^* < 10$, but Linden (1971*b*) has since made direct measurements of the velocity in the fingers which can be used to estimate the fluxes (see (8.3.15)). The results suggest that the conditions in the earlier experiments were unsteady, and that the steady-state flux ratio may be much smaller. Preliminary experiments with layers of sugar over salt solution (Stern and Turner 1969) give a flux ratio of 0.91 in the range $1.05 < R_\rho{}^* < 1.6$, and fingers are clearly a very effective means of transporting *both* components in the vertical. The value of A_2 in this second case ($\tau \approx \frac{1}{3}$) was $A_2 = 10^{-2}$ cm/s, about a tenth of the value for heat–salt fingers.

As yet there is no detailed quantitative theory for the dependence of F_S and F_T on τ. Quite a lot is known, however, about the structure of the fingers through the interface, and this information can be used to support mechanistic arguments which describe the fluxes in an alternative self-consistent way. The 'shadowgraph' picture of

fig. 8.17 pl. XXI obtained by shining a light beam horizontally through an interface containing sugar–salt fingers, shows them to be a regular array of long convecting cells, sharply limited above and below at the edges of the interface, and the same structure has been observed for heat–salt fingers. This is even more graphically illustrated using a colour Schlieren system devised by Shirtcliffe (1972), in which the colour of the image depends on the direction in which light is bent on passing through the tank. This technique shows that the mean density gradient is stable through most of the interface containing fingers, but there is a thin unstable region just at the edges where the fingers break down and feed an unstable buoyancy flux into the convecting layer. A vertical beam of light shone through a thick interface produces a plan view of the fingers (fig. 8.18 pl. XXI) which shows that they tend to be square in cross section, each heavy downward-moving element being surrounded by four in which the motion is upwards (Shirtcliffe and Turner 1970).

With these experimental facts in mind, a region containing steady fingers can be described by the following momentum and diffusion equations:

$$\left.\begin{aligned} \nu\nabla_H{}^2 w &= g(\beta S' - \alpha T'), \\ w\,\partial\overline{T}/\partial z &= \kappa\nabla_H{}^2 T', \\ w\,\partial\overline{S}/\partial z &= \kappa_S\nabla_H{}^2 S', \end{aligned}\right\} \tag{8.3.10}$$

where $\nabla_H{}^2$ denotes $(\partial^2/\partial x^2 + \partial^2/\partial y^2)$, T' and S' are deviations from the horizontal mean and $\partial\overline{T}/\partial z$ is the mean vertical gradient of T. (The close relationship between the physics of salt fingers and buoyancy layers, already remarked on in §8.2.3, becomes apparent when (8.3.10) are compared with (7.4.5) and (7.4.6).) These equations have solutions of the form

$$(w, T, S) = (0, \overline{T}(z), \overline{S}(z)) + (-w_*, T_*, S_*)\sin\frac{x}{L}\sin\frac{y}{L} \tag{8.3.11}$$

provided the amplitudes satisfy relations which are conveniently expressed in terms of the flux ratio

$$F_R = \alpha F_T/\beta F_S = \alpha T_*/\beta S_* = \frac{\kappa_S\alpha\partial\overline{T}/\partial z}{\kappa\beta\partial\overline{S}/\partial z} \tag{8.3.12}$$

as

$$\frac{g\alpha(\partial\overline{T}/\partial z)L^4}{4\kappa\nu} = \frac{F_R}{1-F_R} \tag{8.3.13}$$

and

$$w_* = gL^2\beta S_*(1-F_R)/2\nu. \tag{8.3.14}$$

Notice that (8.3.13) has the form of a Rayleigh number, which is of order one when $F_R \approx \frac{1}{2}$, the value suggested by the experiments on heat–salt fingers. In this case the temperature gradient is observed to be nearly linear through the depth of the interface h; and when the density ratio $R_\rho{}^*$ is large, there is only a small step at the edge, so $\partial\bar{T}/\partial z \approx \Delta T/h$. Thus the width L of the fingers, determined by this large amplitude steady model, is just the same as that found earlier (8.1.13) to be the scale of the fastest growing initial disturbances in a layer of depth h. A constant flux ratio corresponds to a particular value of this Rayleigh number (which again must depend on τ).

In making the above comparison, it has been assumed that the results (8.3.11) to (8.3.14) can be applied within an interface of limited depth, though they are strictly valid only in an unbounded fluid. Now suppose further that S_* is some (specified) fraction of the total step ΔS between the layers and that the system is in a steady state, with the same flux passing through the fingers and the layers. Comparing (8.3.8) and (8.3.14) shows that

$$L \propto (\beta\Delta S)^{-\frac{1}{3}}, \quad w_* \propto (\beta\Delta S)^{\frac{1}{3}}. \tag{8.3.15}$$

We have so far ignored the boundary layer between the finger interface and the convecting layers, where the transition between the two kinds of motion must take place. This is again the least well understood region, though a qualitative description of the processes occurring there is given below.

8.3.4. *The thickness of a 'finger' interface*

The relations (8.3.15) are consequences of two assumptions: that the fluxes should be independent of any external lengthscale (which led originally to the $\frac{4}{3}$ power law), and that all salinity differences are proportional to ΔS (a 'similarity' assumption). They also imply that the interface thickness must be an internally determined quantity, not one which can be arbitrarily imposed: h must in fact be proportional to L, which is clearly consistent with (8.3.13) and (8.3.15) when $\alpha\Delta T \sim \beta\Delta S$. Laboratory measurements in the heat–salt (small τ) case do give values of L consistent with (8.3.13), though there is little evidence to support a simple relation between L and h. Another limit is relevant in the sugar–salt system ($\tau \approx \frac{1}{3}$): as

$\kappa \to \kappa_S$, the appropriate gradient in (8.3.13) becomes the net density gradient or $\Delta\rho/h$ (cf. the remarks at the end of §8.1.3). During the course of an experiment, $\Delta\rho$ changes little because of the nearly compensating fluxes, so $L \propto h^{\frac{1}{2}}$, a result which is in accord with the observations of Shirtcliffe and Turner (1970).

An equivalent prediction that there should be a 'self-determined' interface thickness has been made by Stern (1969) in an entirely different way. He considered the stability of an established field of salt fingers to disturbances in the form of long internal gravity waves, and showed that when

$$\frac{\beta F_S}{\nu\alpha\,\partial\bar{T}/\partial z} \geqslant \text{const (of order 1)} \tag{8.3.16}$$

the disturbances will grow. Thus a given S flux can only be carried by finger convection provided the stabilizing T gradient is large enough. On this view, if an interface is too thick for the imposed $\beta\Delta S \sim \alpha\Delta T$, the fingers will be unstable over a considerable fraction of their length, and the interface must thin. It adjusts itself so that the centre of the interface is near the critical state given by (8.3.16), while at the edges, where $\partial\bar{T}/\partial z$ must initially be smaller, the fingers will still be unstable. Large scale convection should rather abruptly take over the transports here and sharpen the edges, as is indeed observed. The identity of this result with that obtained by the similarity argument is apparent if (8.3.16) is interpreted as a critical Reynolds number of the fingers. With $\beta S_* \sim \beta\Delta S \sim \alpha\Delta T$ and $h \propto L$, it follows that $w_* L/\nu = \text{constant}$ (or more generally, a function of molecular properties alone), which is also implied by (8.3.15).

Given that the flux is proportional to the gradient $\Delta T/h$ across an interface (which holds, with different multiplying constants, in both the finger and diffusive cases), and that the flux ratio is constant, the equilibrium thickness of an interface separating two layers of thickness d is given by

$$F_T = \tfrac{1}{2}d\frac{\mathrm{d}(\Delta T)}{\mathrm{d}t} = a\frac{\Delta T}{h}.$$

Thus

$$h = h_0 + \frac{2a}{d}t, \tag{8.3.17}$$

where a has absorbed several constants of proportionality. This has been obtained without explicitly invoking the flux law (8.3.8), but when that is added (with A_2 constant), it follows that $h \propto (\Delta S)^{-\frac{1}{3}}$, in agreement with (8.3.15). An accurately linear spread of interface thickness in time has been observed in sugar–salt experiments in both the finger and diffusive configurations, so it seems clear that (8.3.17) is not restricted to the similarity (small τ) regime.

When extra mechanical stirring is imposed on each side of a 'finger' interface, the equilibrium is upset and h can even decrease with time. Linden (1971 *a*) has shown also that the fluxes in the heat–salt case change systematically with increasing stirring, between rates corresponding to undisturbed fingers and a purely mechanical transport (see §9.1). Using the difference in turbulent velocity u' across the interface as a measure of the stirring, the criterion for the disruption of the salt finger regime can be expressed as a particular value of the ratio of u' to finger velocity w_*. Using (8.3.14) this can be written alternatively as an internal Froude number based on u', the density difference and the undisturbed interface thickness h. With a steady shear imposed across an interface, on the other hand, the laboratory evidence suggests that the fluxes are changed rather little. Both a stability calculation and direct observations show that, while the cross-stream modes are heavily damped, the down-stream modes are practically unaltered (cf. §7.1.2). That is, the fingers are changed into sheets aligned down shear which can still transport heat and salt efficiently. (See fig. 8.19 pl. XXI.)

8.3.5. *Convection in a region of variable depth*

All the processes considered so far in §8.3 have been essentially one-dimensional, i.e. they have been treated as if they were taking place in a container with vertical walls and constant depth. It will now be shown that the introduction of a sloping boundary can have as important effect: large scale circulations can then be driven by a uniform flux imposed over a horizontal surface. The idea is applicable however this flux is supplied (for example, it could be due to a uniform cooling at the surface), but it arises in the context of double-diffusive convection and is conveniently described here. It is quite different from the weak local effects of a sloping boundary

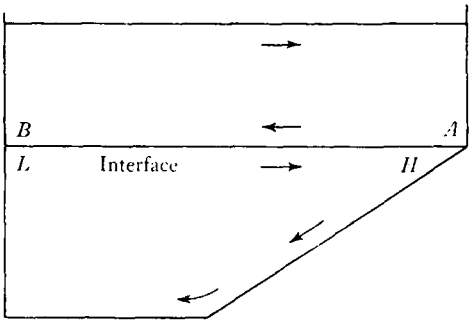

Fig. 8.20. Sketch of the motions produced in a container with a sloping boundary, by a flux of buoyancy across an interface.

described in §8.2.3; the effect to be considered now is a purely geometrical one.

The essential point is contained in the equations (8.3.7). The rate of change of density of a fluid layer, for a given flux, depends inversely on the depth. In the configuration sketched in fig. 8.20 the fluid at H will become heavier faster than that at L. A horizontal pressure gradient is set up, which drives a circulation in the sense shown, including a flow right down the slope to the bottom. At the same time the flux across the interface at the corner will be reduced because of the decreased concentration difference there, and the fluid at A will get lighter more slowly than at B. This sets up a circulation in the same sense (even with an upper layer of uniform depth) and there is a strong shear across the interface.

These circulations have been observed in the laboratory with sugar–salt layers set up in both the diffusive and finger senses. With a finger interface, the flow down the slope is quite thin and rapid. The growing pool of fluid at the bottom is stably stratified (cf. §7.3.3), but shows a notable absence of fingers; in fact a series of sharp 'diffusive' interfaces is produced, since the relative concentrations are reversed in this region (see fig. 8.21 pl. XXII). With salt above sugar, on the other hand (a diffusive interface), the bottom layer and the slope current show a secondary finger effect. A tentative application of the idea has been made by Gill and Turner (1969) to the formation of bottom water in the Antarctic ocean, where warm salty intermediate water underlies colder fresher water.

The Antarctic situation is ambiguous, because cooling and

freezing at the surface can also produce a downward flux of buoyancy. But in this case too the depth variation will be important, with the densest water forming on the shallow shelf and tending to flow down the slope (subject to the constraint of the earth's rotation which must be important in the oceanic case). Similarly, any process which increases the density, such as uniform cooling at the surface, could have an important effect on currents at other coastlines, just because of the change in depth through which mixing can occur.

The depth changes need not be smooth for the same argument to apply; a step is equally effective. If a constant buoyancy flux is imposed at the surface of a fluid in a region consisting of a long shallow arm, connected to a deeper reservoir, then a circulation is set up with an inflow at the surface and an outflow along the bottom of the shallow region. One can in this way realize in the laboratory a flow which resembles the similarity solution described in §5.3.4 (see fig. 5.14).